Available online at www.jrors.ir

Journal Of Radar and Optical Remote Sensing

JRORS 2 (2019) 61–74

Using EO1 Hyperspectral Images for Geological Units Mapping

Ali Asghar Torahi [a*], Parisa Safarbeyranvand[b], Hasan Hasani Moghaddam[b], , Parviz Ziaeian Firoozabad[c], Ali Hoseeingholizade[d]

[a] *Assistant Professor Remote Sensing and GIS, Kharazmi University of Tehran.*

[b] *Master of Remote Sensing and GIS ,Kharazmi University of Tehran.*

[c] *Associate Professor of Remote Sensing and GIS, Kharazmi University of Tehran.*

[d] *PhD Student of Remote Sensing and GIS, University Tehran.*

Received 21August 2019; revised 6 September 2019; accepted 15 September 2019

Abstract

The issue of mapping geological units during an evolving process has now reached a point where the detection and classification of geological units is carried out with the aid of hyperspectral sensing. In this study, using hyperspectral image of Hyperion sensor, related to Khorramabad area in Lorestan province, and using Spectral Angle Mapper (SAM) and SVM (Support Vectors Machine) algorithms for detecting and separating geological units after performing the necessary preprocesses, the MNF conversion and PPI algorithm were used to reduce data and extract pure pixels on the image, respectively. From overlapping of pure pixels with geological units and ground data, the average range for each member was extracted and then these net members were used as inputs for the above mentioned algorithms and class B DVD image was done. Field surveys performed at the points provided by the Spectral Angle Mapter (SVM) confirm the superiority of the SVM method in separating geological units. Finally, by verifying the accuracy of the algorithms by calculating the error matrix, the accuracy of the classification of each method are (68.83) and (81.70), for SAM and SVM respectively it was found that at the end of the SVM algorithm with a total accuracy of 81.70 was introduced as the best classification algorithm.

Keywords: Hyperspectral Images, Geological Plot Map, Pure Members, SAM, SVM.

[*] Corresponding author. Tel: +098-9197951476.
Email address: atorahi@khu.ac.ir.

1. Introduction

Using remote sensing technology and using satellite data reduced the costs and increased accuracy and speed of data collecting (Alvipanah, 2013). The use of satellite technology in the last decades as one of the most important means of information acquisition attracted the attention of many experts and specialists of various sciences, including geology, mining, environment, meteorology, agriculture and etc. From years of 1980, by introducing of Hyper-spectroscopic sensors, a major step has been taken in the area of remote sensing technology (Hasani Moghaddam, 2019). Hyper-spectral sensors, in comparison with multi-spectral sensors, produce much more accurate spectral data and therefore allow for more accurate identification of ground targets (Campsvalls et al., 2014). As the Hyper-spectral sensors are used of bands extremely large spectra produce a large amount of spectral data, so it is also necessary to use methods that are capable of processing and extracting valuable information from this high dimension data. The relationships of geological and remote sensing are nearly thirty years old (Waske et al., 2009). In the most hyper spectral sensors, reflection measurements of surface phenomena with a spectral width of 0.01 μm and spectral ranges of 0.4 to 2.5 μm are acquired, so this property makes it possible for geological unit's investigations. The existing maps of the geological units are prepared by traditionally ways; in this research, used of remotely sensed hyperspectral images to produce more accurate maps of geological units. The data obtained from the measurements in terms of providing a wide coverage of the area and providing quantitative parameters can be a suitable source for updating geological maps (Rajendran et al., 2007). Images from remote sensing technology provide efficient data that requires processing on the image to extract information from them. Among different methods of remote sensing, the classification techniques have a special role in analysing, separating and detecting various geological units. Image classification is one of the main process components of the information extracting from an object that are obtained by examining the relationship between spectral effects and classes (Oommen et al., 2008).

Ramakrishnan and Bharati (2015), review the potential of Hyperspectral Remote Sensing (HRS) technique in various geological applications ranging from lithological mapping to exploration of economic minerals of lesser crustal abundance. This work updates understanding on the subject starting from spectroscopy of minerals to its application in exploring mineral deposits and hydro-carbon reservoirs through different procedures such as atmospheric correction, noise reduction, retrieval of pure spectral endmembers and unmixing. Besides linear unmixing, nonlinear unmixing and parameters attributed to nonlinear behaviour of reflected light are also addressed. A few case studies are included to demonstrate the efficacy of this technique in different geological explorations. Finally, recent developments in this field like ultra-spectral imaging from unmanned aerial vehicles and its consequences are pointed out.

Kurz et al. (2017), developed a novel geological mapping technique for subsurface construction sites. A major result of this work is that the use of artificial halogen light sources, at ranges suitable for imaging rock faces of similar size to the TT-Niche, is possible and allows good quality hyperspectral data to be obtained. The importance of this result must be stressed, as there were many uncertainty factors with respect to the strength, emitted wavelengths and stability of the required light sources prior to the start of the study. Although complex illumination variations were present in the data, especially at long range, due to the number and configuration of lights used, the data quality was suitable for mapping the large scale geology.

Blackburn (2007), appraised the developing technologies and analytical methods for quantifying pigments nondestructively and repeatedly across a range of spatial scales use of hyperspectral remote sensing. The results of this study showed that hyperspectral images is a better way for evaluating pigments ranges and it can be used in agriculture, forest, environmental, Eco physiological and etc.

Bordoloi et al. (2013), for involving a pot experiment with twenty acidic soils varying widely in properties, evaluated six chemical indices of soil N-availability. Of all the indices evaluated, PBB-N showed the best correlation with plant parameters. Based on the highest correlation of PBB-N with biological indices as well as plant responses, they proposed PBB-N as an appropriate singular of N-availability in the acidic soil of India and other regions with similar soils.

Torahi and Rai (2011), developed a methodology to map and monitor land cover changes using multi temporal Landsat TM and ASTER data. Their data classified into forestland, rangeland, water bodies, agricultural lands and residential area. The MLC algorithm was used and results evaluated by collected GCP. Results showed that image classification of Zagros mount by satellite data have good results in order to ground studies.

This research tries to increase the accuracy of Geological maps by classifying and detecting on the basis of the obtained spectra to identify geological units with the help of satellite images of Hyperion.

2. Study Area

The study area is located at the west of Iran, Lorestan province, Khorramabad city. Khorramabad is geographically located at 33 degrees, 29 minutes north latitude and 48 degrees, 21 minutes east.

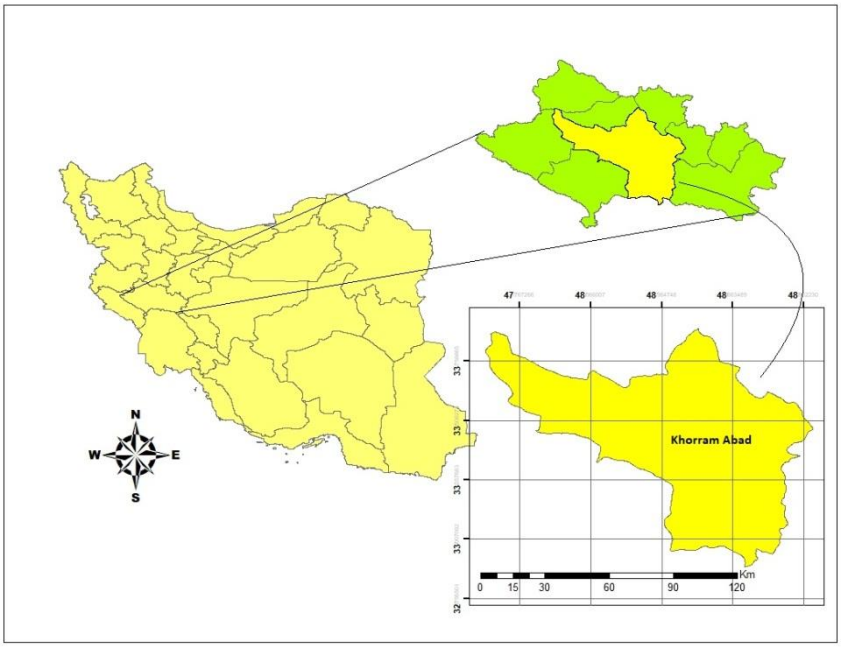

Figure1. Geographic location of study area

The sedimentary status of the province shows this fact that different parts of it during the course of time, have different geological characteristics and differentiated from each other. Therefore, considering tectonic activities and building styles of different units of age, units or sedimentary basins and types of sediments related and also magmatic and metamorphic activities of Lorestan province based on geological and structural units of Iran in two zones are as follows:

A) Zagros Zone**:** wrinkled Zagros Sub-Zone – high Zagros Sub-Zone

B) Sanandaj-Sirjan Zone

In the studied area, we describe the characteristics of the units that are outcropping in the area, including the stone units of the Gachsaran, Sarvak, Bakhtiari, Asmari, Keshkan units.

Table 1. The introduction of the most important available lithology units (studied goals) in the studied zon

No	sign	Lithology
1	PIbk	Cement conglomerate with intense alteration and slightly weathered sandstone with cross- stratification
2	Mgs	Anydrite, salt, red and gray marl of bamiyan plasters, argillite lime and limestone (Gachsaran unit)
3	Emassb	Seperated stenes of Shahbazan and Asmari Units
4	ReKn	Red conglomerate, siltstone and sandstone (Kashkan unit)
5	Ksv	Gray limestone, dolomitic lime

3. Materials and Methods

3.1. Satellite Image of EO-1 Hyperion Sensor

The image used in this study was captured in September 5, 2010, with a route number 166 and a row number 37. Its dimensions are 7.65 km wide and 185 km long. The centre of this area is the coordinates of 31 ° 37'00.09 "north and 47 ° 53'19.11" east.

3.2. Preprocessing satellite data

The preprocessing operations required for data preparation include two general stages of radiometric correction and geometric correction. One of the corrections for Hyperion data is the correction of the spectral curvature in the image, which is due to the push broom technology of imaging has been developed in all Hyperion data (Sidine et al., 2014). Correction of this error was done by means of modulating the mean of the column in the radiative space in the ENVI software. In this method, for each single band of Hyperion data, the mean value of each column is equal to the average value of the band. Vertical stripes are other errors in Hyperion images that were repaired using the De-stripping method. The image data, which was digital, was first converted to radiance and then to reflection. The digital values of Hyperion Level 1 products were 16-bit radiants. VNIR[2] bands have a scale factor of 40 and SWIR[3] bands have a scale of 80. Thus, according to the relation, radian values for the bands of this image were corrected:

VNIRL: Digital Number/40
SWIRL: Digital Number/80

Atmospheric correction converts radian values to reflection values in pixels. Reflection information in comparison with radiance, because reflective information is relatively similar in everywhere in the world and depends on the characteristics of each substance; while radiance information is different, it is affected by various atmospheric indices. Hyperion image correction and radionuclide conversion to reflection were performed using the FLAASH[4] atmospheric correction pattern.

After radiometric correction, geometric correction was applied on the images. For geometric correction, images of ground control points such as intersections of roads and roads that were clearly visible in both the Hyperion and ALI satellite imagery were selected. After these two stages, the image was prepared for performing research methods.

3.3. Image Processing

After performing the preprocessing and geometric and atmospheric correction, the reflection image should be entered into the processing stage and extracted the required information, which is presented below:

3.4. Select a Band

Of the 242 Hyperion spectral band used in this study, 196 are calibrated and unique. If we eliminate water absorption bands and visualize and eliminate the bands that are rich in noise, then 5 15 bands will be processed into the processing stage.

---

2 Visible-near infrared
3 Short wave infrared
4 Fast Line-of-sight Atmospheric Analysis of Spectral Hypercubes

Table2. Acceptable bands which enter processing

Acceptable bands	Spectral range
8-57	VNIR range
79	SWIR range
83-119	
133-164	
183-184	
188-1220	

3.5. Minimum Noise fraction (MNF)

The use of metaphysical data needs to reduce noise and data dimensions. The MNF conversion is considered as a noise reduction transformer. This conversion is a linear transformation used to determine the dimension and size of the image, to separate the noise from other information, and reduce the processing speed at a later stage. In this conversion, the image is first converted into two parts of noise and non-noise, and then the non-noise part is recognized as the main component and noise is eliminated (Rangzan et al., 2011).

3.6. Pixel Purity Index (PPI)

The PPI algorithm is used to find pixels that have higher purity (end pixels) in over-spectral images. For this purpose, gave 10 of the first output bands of MNF transformation, which is non-noise, as input to the PPI algorithm, and the output of this algorithm is the image that identifies the pure pixels.

3.7. Extracting the Reference Spectrum (Endmember)

Many of the classification algorithms in ultra-spectral images require the introduction of spectral features of the members (to each class or the objects that are classified or detected in the metaphysical image) to begin processing.

3.8. Extraction of Endmembers by Identifying Pure Pixels

The Endmembers were extracted from the areas where the geological unit was identified. With 4 steps of field review and field mapping and geodetic coordinates registration using a high precision GPS device and using sampling points that were matched to the pure pixels extracted from the PPI algorithm, were able to extract the reference range of the units from the image itself and this reference spectrum was used as input for classification algorithms.

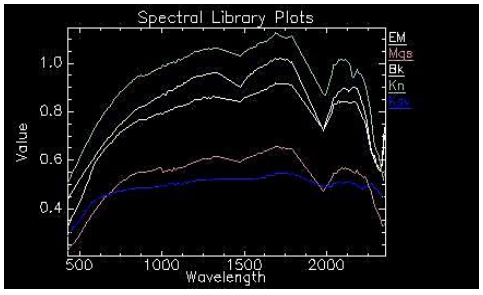

Figure2.The spectra extracted from the image of the geological units of the region

3.9. Ground Control Point

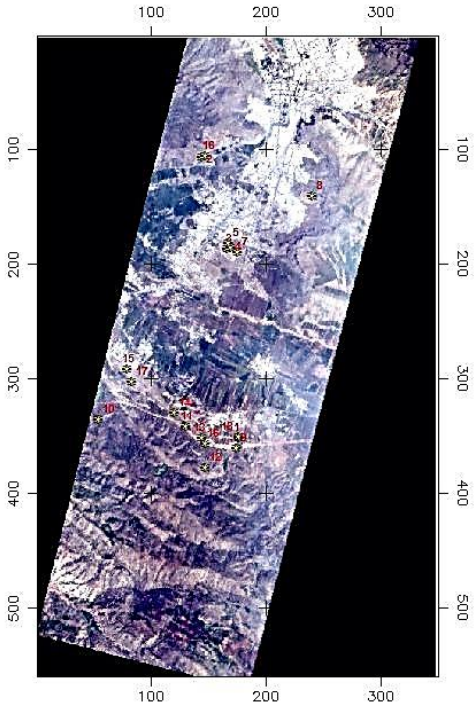

Figure3. Location of samples taken from the study area

Table3. A number of sampling points

x	y	Zone	Formation	num
252771	252771	39	Sarvak	1
251385	3706698	39	Sarvak	2
251283	3706647	39	Sarvak	3
252558	3696929	39	Sarvak	4
252191	3703667	39	Sarvak	5
252174	3703477	39	Sarvak	6
252261	3703520	39	Sarvak	7
247732.95	3697558	39	Kashkan	8
250744.32	3697341.14	39	Kashkan	9
252493	3696589	39	Kashkan	10

251411	3696741	39	Asmari	11
248699	3699299	39	Asmari	12
250348	3697816	39	Asmari	13
251284	3696918	39	Asmari	14
251407	3695915	39	Asmari	15
248854	3698895	39	Gachsaran	16
252558	3696929	39	Bakhtiari	17
252549	3696968	39	Bakhtiari	18

3.10. Used Methods

3.10.1. Spectral Angle Mapper (SAM)

Spectral Angle Surveyor as a Guided Classification Method an Effective Method for Spectrum Comparison Images are relative to the standard range or reference spectrum. The algorithm of this method calculates the similarity between the two spectra by the spectral angle between the two. In fact, by transforming the spectra into a vector in space, the size of the number of bands, the angle between the two vectors is calculated. In this method, for calculating the angle, the direction of the vectors is important and not their length, and therefore the pixel brightness does not affect its classification. The angle between 0 and 1 if below, the more accurate it will be. If the angle is one, the entire image is identified as the phenomenon. For example, to compare a pixel, the desired pixel spectrum with the same pixel spectrum is plotted between the reference spectra on two bands in a coordinate axis. The resulting points are then drawn to the origin and the angle between the two resulting lines is known as the pixel identification angle. To obtain the angle α between two vectors

$$\alpha = \cos^{-1}\left[\frac{\vec{r}.\vec{t}}{\|\vec{r}\|.\|\vec{t}\|}\right] \quad (2)$$

That way, it can also be written

$$\alpha = \cos^{-1}\left[\frac{\sum_{i=1}^{nb} t_i r_i}{\left[\sum_{i=1}^{nb} t_i^2\right]^{\frac{1}{2}}\left[\sum_{i=1}^{nb} r_i^2\right]^{\frac{1}{2}}}\right] \quad (3)$$

In this formula:
bn: number of bands
ti: spectrum tested
ri: reference spectrum

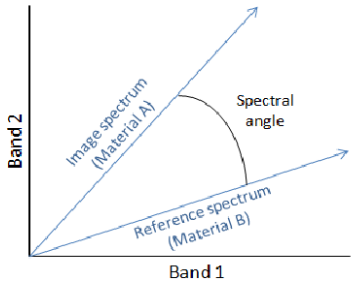

Figure4. The spectra of the tested spectrum and the standard range in the SAM process

The most important advantage of the SAM algorithm is its simplicity of structure and rapid use to display the spectral similarity between the image spectrum and the reference spectrum. The classification problem using this algorithm is not considering the problem of mixed pixels(Fahimnejad et al., 2007).

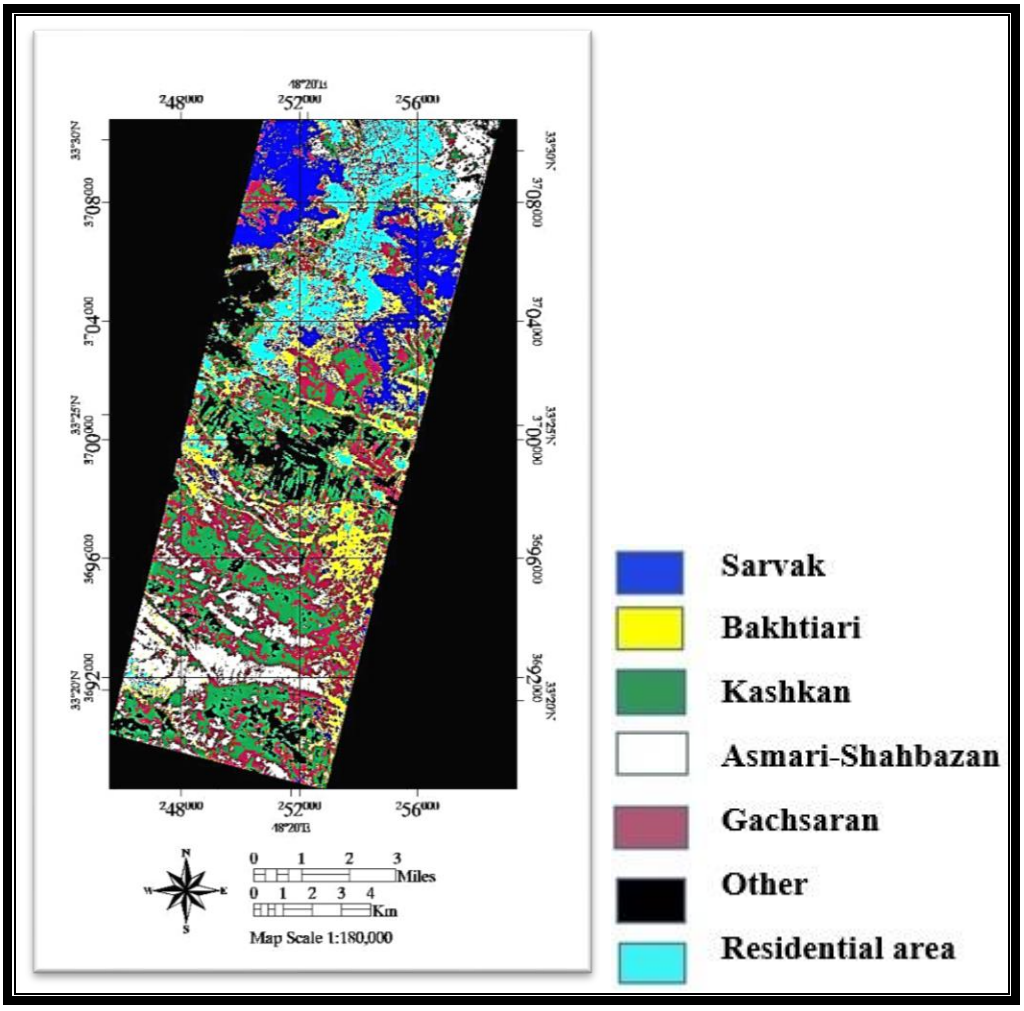

Figure5. Classification result with SAM algorithm

3.10.2. Support Vector Machine (SVM)

Support vector machine is a useful technique for data classification(Abbasi et al., 2015). A classification

task usually involves separating data into training and testing sets. Each instance in the training set contains one "target value" (i.e. the class labels) and several "attributes" (i.e. the features or observed variables). The goal of SVM is to produce a model (based on the training data) which predicts the target values of the test data given only the test data attributes(Wei Hsu et al., 2003).

Given a training set of instance label point $(x_i, y_i), i = 1,...,l$ where $x_i \in R^n$ and $y \in \{1, -1\}^l$, the support vector machine(SVM) require the solution of the following optimization problem:

$$\min_{w,b,\xi} \frac{1}{2} w^T w + C \sum_{i=1}^{l} \xi_i$$
$$\text{Subject to } y_i (w^T f(x_i) + b) \geq 1 - \xi_i, \quad (4)$$
$$\xi_i \geq 0.$$

Here training vectors x_i is mapped into a higher (maybe infinite) dimensional space by the function ϕ. SVM finds a linear separating hyperplane with the maximal margin in this higher dimensional space. $C > 0$ is the penalty parameter of the error term. Furthermore, $K(x_i, x_j) = f(x_i)^T f(x_j)$ is called the kernel function. Though new kernels are being proposed by researchers, beginners may find in SVM books the following four basic kernels:

- Linear: $K(x_i, x_j) = x_i^T x_j$.
- Polynomial: $K(x_i, x_j) = (\gamma x_i^T x_j + r)^d, \gamma > 0.$
- Radial Basis Function(RBF): $K(x_i, x_j) = \exp(-\gamma \| x_i - x_j \|^2), \gamma > 0.$
- Sigmoid: $K(x_i, x_j) = \tanh(\gamma x_i^T x_j + r).$

Here, γ, r are kernel parameters.

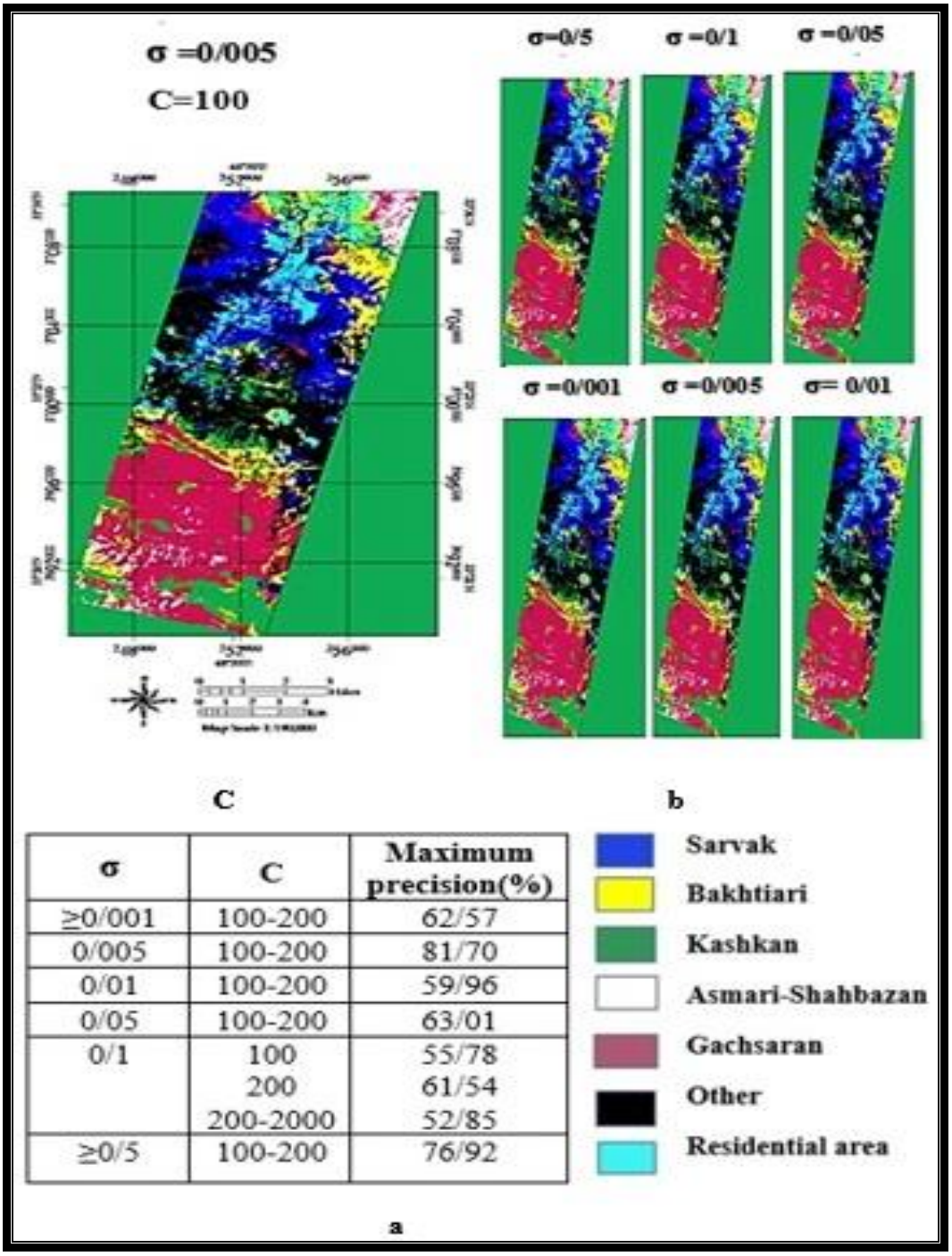

σ	C	Maximum precision(%)
≥0/001	100-200	62/57
0/005	100-200	81/70
0/01	100-200	59/96
0/05	100-200	63/01
0/1	100 200 200-2000	55/78 61/54 52/85
≥0/5	100-200	76/92

***Figure* 6.** (a)Validation results for obtaining the best values of the SVM variables are σ and C .Maps of geological units of the region Studies for: (b) optimal amounts; and (c) varying amounts of variables

4. Results And Discussion

After compilation of classified pictures, to assess the accuracy of each method, the GPS points taken by ground observations were used as ground maps to determine the accuracy of the error matrix, the accuracy of classification in each method, and ultimately the best way to estimate the geological map of the units Introduced. The results of a health assessment are usually presented as an error matrix, whereby a variety

of parameters and values representing accuracy or some kind of error in the results are extracted from this matrix. This matrix is the result of a comparison of the pixels to the pixels, the pixels defined with the corresponding pixels in the classification results. In the error matrix, land data in the columns and data related to the classification results are given in the rows of this matrix. The numbers on the matrix's main diameter indicate the number of pixels whose labels match the two sets of data or, in the other hand, the number of pixels that are correctly categorized over this diameter. Non-diagonal elements are the set of errors. Based on the error matrix, several parameters are extracted for accuracy and error.

In this study, the results of the evaluation are presented as general and Kappa coefficients; the overall accuracy is the average of the accuracy of the classification, which represents the ratio of the correct pixels classified to the total of the pixels in question. The Kappa coefficient calculates the classification accuracy in a completely randomized manner, which means that the kappa gives the classification accuracy as compared to the state of a completely randomized image (Richard, J.A, 1995).

$$O.A = \frac{\sum_{n=1}^{c} E_{ii}}{N} \times 100 \quad (5)$$

C: number of classes
N: total number of pixels determined
Eii: Diameter members of the error matrix
The ratio of the calculation of this coefficient is as follows:

$$k = \frac{N\sum_{i=1}^{r} x_{ii} - \sum_{i=1}^{r}(x_{i+} * x_{+i})}{N^2 - \sum_{i=1}^{r}(x_{i+} * x_{+i})} \quad (6)$$

In this case, N is the total number of pixels of the ground plane, + xi the sum of the elements of the row i and + i is the sum of the elements of column i.

These algorithms were compared and verified in the classification of ultra-spectral images. The SVM algorithm has the highest accuracy (overall accuracy of 70/81 percent and kappa coefficient of 72/0) in classification and SAM algorithm with high accuracy (overall accuracy of 68/83 percent and Kappa coefficient was 0.49) but less than SVM algorithm. One of the influential issues in the SVM results is to allocate appropriate values to its variables, which was used for mutual validation.

The results showed that, by assigning optimal values to the variables c and σ, SVM has a high ability to classify the geological units of the region. However, the inappropriate values of these variables can greatly affect the classification accuracy.

After determining the optimal values for the variables c and σ, these values were used for SVM training. Finally, the SVM was trained to classify the study area. Because of the wide range of variable c as desirable values of 200-1000, and yet, the results are not very large, the only geological maps of the region for the values of c = 100 and 005 / σ = 0 are shown in Fig. 13-13 (b). Is.

Table4. Error matrix, general accuracy, and kappa coefficients for the results of the SAM algorithm

Class	**Ground data (experimental pixels)**						
	Sarvak	Gachsaran	Asmari	Kashkan	Bakhtiari	Residential	Full pixels
Not classified	0.44	1.40	1.40	0.00	4.24	1.35	0.86
Sarvak	79.96	3.17	0.45	0	8.93	3.71	54.95
Gachsaran	2.88	31.81	9.75	17.47	12.75	1.05	9.18
Asmari	6.08	4.42	71.27	0	17.13	1.1	3.83

Kashkan	0.00	0.85	0	55.08	5.08	0	4.27
Bakhtiari	5.57	11.66	11.82	1.01	56.93	4.9	11.91
Residential	3.71	1.05	1,10	0	4.90	93.31	4.80
others	3.34	22.89	0	34.74	6.76	0	10.2
Full pixels	100.00	100.00	100.00	100.00	100.00	100.00	100.00
Kappa coefficient : 0.49					**Total accuracy : 68.83**		

Table5. Error matrix, general accuracy and kappa coefficient for the results of the SVM algorithm

Class	**Ground data (experimental pixels)**						
	Sarvak	Gachsaran	Asmari	Kashkan	Bakhtiari	Residential	Full pixels
Not classified	0.00	0.00	0.00	0.00	0.00	0.00	0.00
Sarvak	69.17	0.01	0.00	0.39	0.00	0.00	24.75
Gachsaran	3.35	95.20	39.23	0.78	5.07	0.00	49.72
Asmari	0.03	4.74	59.83	3.29	11.66	0.00	8.86
Kashkan	0.02	0.00	0.20	89.53	1.01	0.00	2.03
Bakhtiari	7.70	0.05	0.75	4.07	81.08	0.00	4.93
Residential	3.21	0.00	0.00	0.19	0.84	100.00	2.15
others	16.51	0	0	1.75	0.34	0	7.56
Full pixels	100.00	100.00	100.00	100.00	592	100.00	100.00
Kappa coefficient: 0.72					**Total accuracy: 81.7**		

The evaluation of the results of this study shows that the mapping of geological units mapped using SAM and SVM algorithms was carried out using maps previously provided by Geological Survey of Lorestan province and Geological Survey.

The country that provided the fact that the SVM algorithm with a general accuracy of 81.70% and a kappa coefficient of 0.72% were more accurate than the SAM algorithm with a total accuracy of 68.63% and a coefficient of 0.44%, respectively(Table 3 and 4). Also, the results show that the SVM algorithm, taking into account the regional conditions, is an effective method for classifying the region based on existing geological units in geological mapping research. Due to the large capability of images in the resolution of phenomena, it is shown that the identification and separation of geological units using these images is easier and more accurate than other methods, such as the use of multidimensional images.

Table6. Area of geological units using the algorithm used

Algorithm / Formation	SAM	SVM
Sarvak	2304.09	2523.69
Gachsaran	4387.32	4447.44
Asmari	1699.47	762.39
Kashkan	1984.59	16257.42
Bakhtiari	2371.05	1793.25

According to the results of calculating the area of different formations in the study area (see 5), the Kashkan Formation has the highest calculated area by the SVM class and Gachsaran Formation with the highest calculated area in the SAM classification method.

The accuracy of the detection of Sarvak, Gachsaran, Asmari, Kashkan and Bakhtiari formations by SAM and SVM algorithms is shown using the results of tables (4), (5) in the chart 6.

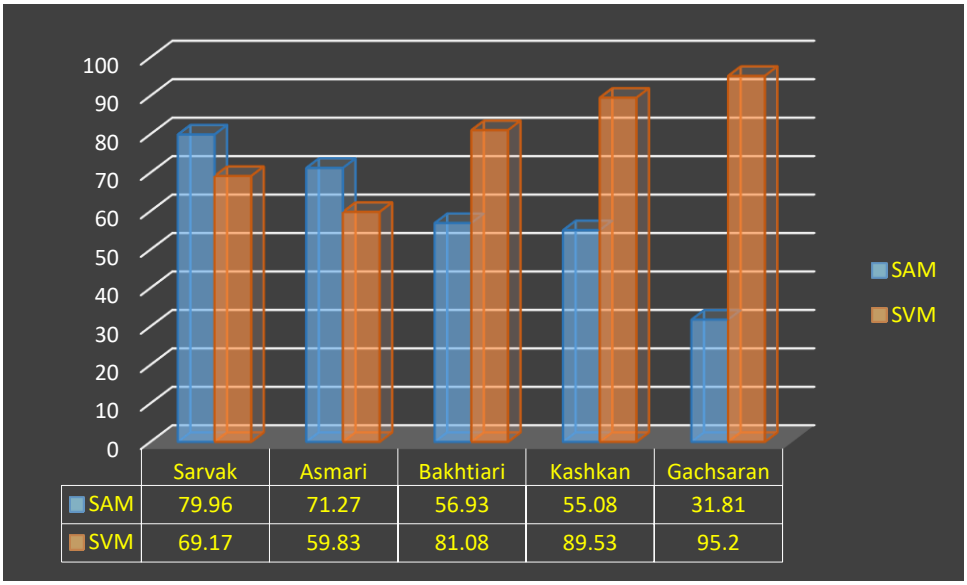

Figure7. Comparison of the accuracy of the different formations detection by classification algorithms

It is suggested that in future investigations, more powerful geodetic sensors than Hyperion (with a pixel size of 30 meters) are used to identify valuable geological units in order to produce higher precision maps.

5. Conclusion

The geological mapping over the years and extensive studies and studies has already reached the point that, instead of being in the field and doing fieldwork and spending a lot of time and money, using the science of measuring and using metaphysical images in It can be done in a short time and with high precision.

In this research, SAM and SVM algorithms were used to identify geological units. One of the most important factors in the target's detection that affects the final evaluation of the algorithms is the choice of the threshold value that was determined by trial and error in this study. For better identification of geological units, we used MNF, PPI based on SVM and SAM composite. SVM classifier because of its kernels that used, has a better results. It may be its inner principal and its capabilities for identification of complex units. Because of SVM save boundaries of clases as well as, so it is usefull for classification and extraction of geological units. In this classification, in compariosion of SAM classifier that only uses of spectral similarity

method for classes distinguishing, information of spectral and pixel location are key factors to pixels label.

References

Abbasi, B., Arefi, H., Bigdeli, B., & Roessner, S. (2015). Automatic generation of training data for hyperspectral image classification using Support Vector Machine, *36th International Symposium on Remote Sensing of Environment, Berlin*, Germany.

Blackburn, G, E. (2007). Hyperspectral remote sensing of plant pigments, *Journal of experimental botany*, Vol (58), pp. 855-867.

Bordoloi, L, J., Singh, A, K., Kumar, M., Patrisam., & Hazarika, S. (2013). Evaluation of nitrogen availability indices and their relationship with plant response on acidic soils of India, *Plant soil environ*, Vol (59), pp. 235-240.

Hsu, C, W., Chang, C. C., & Lin, C, J. (2003). A practical guide to support vector classification.

Torahi, A, A., & Rai, S, Ch. (2011). Land Cover Classification and Forest Change Analysis, Using Satellite Imagery - A Case Study in Dehdez Area of Zagros Mountain in Iran. *Journal of geographic information system*, Vol (3), pp. 1-11.

Fahimnejad, H. (2007). Resolution evaluation of Agriculture Products by Remote Sensing Data (Hyperion hyperspectral sensor). *M.A thesis, surveying college.Khaje Nasiraldin Tosi University*.

Kurtz, T.H., Buckley,S,J., & Becker,J,K.(2017). Hyperspectral imaging: a novel geological mapping technique for subsurface construction sites. *Proceeded of the world tunnel congress 2017*. Surface challenges, Bergen. Norway.

Rangzan, K., Saberi, A., Jokar, E., & Mohamadian, F (2011), Identification and Estimation of Area under Cultivation of Agriculture land by Hyperion sensor data, *Geometric Conference 90*.

Ramakrishnan, D., & Bharti. R. (2015). Hyperspectral remote sensing and geological applications. *Current science.No.5*, pp.879-891.

Seyyedin, A. Oil (hydrocarbon) span detection by detection methods in hyperspectral mages. *M.A thesis. Remote Sensing, GIS*, Tehran University.

Sharifi, A.R. (2008). Classification of Hyperspectral Images by Analyzing Spectral Signatures of Phenomena. *Master's Thesis, Field Student, and GIS*, Tehran University.

Alvipana,S.K (2013). "application of Remote Sensing in Geology" 4thversion, Tehran. Tehran press. Hypersp». *Scientific promotional journal.Oil and Gas Detection & protection*.No.111, p.6-690.

Camps-Valls, G., Tuia, D., Bruzzone, L., & Benediktsson, J. A. (2014). Advances in hyperspectral image classification: Earth monitoring with statistical learning methods. *IEEE Signal Processing Magazine*, 31(1), 45-54.

Chang, C.I. (2003). Hyperspectral Imaging: Techniques for spectral Detection and Classification, Orlando. FL:Kluwer Academic.

Hasani Moghaddam, H., Torahi, A. A., & Zeaiean Firooz Abadi, P. (2019). Using discrete wavelet transform to increase the accuracy of hyperspectral and high resolution images fusion. *JRORS*, 1, pp. 22-30.

Chen, X., Warner, T. A., & Campagna, D. J. (2007). Integrating visible, near-infrared and short-wave infrared hyperspectral and multispectral thermal imagery for geological mapping at Cuprite, Nevada. *Remote Sensing of Environment*, 110(3), 344-356.

Oommen, T., Misra, D., Twarakavi, N. K., Prakash, A., Sahoo, B., & Bandopadhyay, S. (2008). An objective analysis of support vector machine based classification for remote sensing. *Mathematical geosciences*, 40(4), 409-424.

Rajendran, S., Srinivasamoorthy, K. & Aravindan, S. (2007). Mineal exploration: recent strategies. *New India Publishing*, 528.

Richards, J. A., & Jia, X. (1999). Remote Sensing Digital Image Analysis–Springer. Berlin, Germany.

Shrestha, D. P., Margate, D. E., Van der Meer, F., & Anh, H. V. (2005). Analysis and classification of hyperspectral data for mapping land degradation: An application in southern Spain. *International Journal of Applied Earth Observation and Geoinformation*, 7(2), 85-96.